Laser and Particle Beams (2017), *35*, 294–303.
© Cambridge University Press, 2017 0263-0346/17
doi:10.1017/S0263034617000179

Laser-generated plasmas by graphene nanoplatelets embedded into polyethylene

L. TORRISI,[1] G. CECCIO,[1] N. RESTUCCIA,[1] E. MESSINA,[2] P. G. GUCCIARDI,[2] AND M. CUTRONEO[3]

[1]Dip.to di Scienze Fisiche MIFT, Università di Messina, V.le F.S. D'Alcontres 31, 98166 S. Agata, Messina, Italy
[2]IPCF-CNR, V.le F.S. D'Alcontres 37, 98166 Messina, Italy
[3]Nuclear Physics Institute, CAS, 25068 Rez, Czech Republic

(RECEIVED 14 October 2016; ACCEPTED 20 February 2017)

Abstract

Graphene micrometric particles have been embedded into polyethylene at different concentrations by using chemical–physical processes. The synthesized material was characterized in terms of mechanical and optical properties, and Raman spectroscopy. Obtained targets were irradiated by using a Nd:YAG laser at intensities of the order of 10^{10} W/cm^2 to generate non-equilibrium plasma expanding in vacuum. The laser–matter interaction produces charge separation effects with consequent acceleration of protons and carbon ions. Plasma was characterized using time-of-flight measurements of the accelerated ions. Applications of the produced targets in order to generate carbon and proton ion beams from laser-generated plasma are presented and discussed.

Keywords: Advanced targets; Au NP; Graphene; Laser-generated plasma; Time-of-flight measurements

1. INTRODUCTION

Graphene is a material constituted by planar carbon atoms with peculiar properties such as mechanical, thermal (Balandin *et al.*, 2008; Balandin, 2011), electrical (Novoselov *et al.*, 2005), and optical (Bonaccorso *et al.*, 2010).

Atoms in graphene are sp^2 hybridized and form hexagons with 120° angles with two-dimensional (2D) properties. The presence of defects generated pentagons, hexagons, and fullerenes. Carbon nanotubes can be considered as graphene cylinders with single or multiple walls. Graphene has optimal electrical conductivity, showing an electronic mobility above 2×10^5 cm^2/V·s (Bolotin *et al.*, 2008), small absorption of the visible radiation (2.3% per layer) (Nair *et al.*, 2008), which is shiftable on doping by different atomic species (Al, Cu, Ti, etc.).

It has high mechanical resistance to strength and flexibility, with an ultimate tensile strength of 130 GPa, higher with respect to stainless steel, a density of about 1.75 g/cm^3, lower with respect to the graphite, and a thermal conductivity of about 600–5000 W/mK range with theoretical predictions going up to 10,000 W/mK (Balandin, 2011). The liquid phase exfoliation (LPE) of graphite to give graphene is one of the most promising ways to achieve large-scale production at an extremely low cost (Yu *et al.*, 2015). The production of composite materials, such as those based on polymers enriched with graphene, permits to modify the chemical and physical properties of the materials. New polymers can be realized with peculiar properties concerning their electrical and thermal conductivity, optical characteristics, mechanical properties, chemical reactivity, and others (Hasan *et al.*, 2009; Rafiee *et al.*, 2009; Kuilla *et al.*, 2010; Shahil & Balandin, 2012; Messina *et al.*, 2016).

In the field of laser-generated plasma in vacuum a special interest is devoted to the use of materials with advanced mechanical, optical, and electrical properties. Particularly important is the case of polyethylene (PE)-based materials to produce plasma rich in hydrogen and carbon ions. Nano- and sub-nanosecond laser pulses, at high-intensity, permit to produce non-equilibrium plasma from laser–matter interaction in vacuum. The high-charge separation effects in such non-equilibrium processes generate non-isotropic, very high electric fields from which ions and electrons can be accelerated. The acquired particle energy has directive velocity, mainly along the normal direction to the target surface, whose characteristics depend strongly on the chemical and physical properties of the laser-irradiated target (Torrisi *et al.*, 2015*a*). The optical and electrical properties of the target, for example, influence the penetration depth of the

Address correspondence and reprint requests to: L. Torrisi, Dip.to di Scienze Fisiche MIFT, Università di Messina, V.le F.S. D'Alcontres 31, 98166 S. Agata, Messina, Italy. E-mail: lorenzo.torrisi@unime.it

https://doi.org/10.1017/S0263034617000179 Published online by Cambridge University Press

laser in the polymer and the electron density of the produced plasma (Eliezer, 2002). Moreover, the target thickness and the mechanical strength influence the electron and ion accelerations from the non-equilibrium plasma, both in terms of kinetic energy and angular distribution, as well as directionality of the emitted ions and possible deformation of irradiated thin foils (Zeil *et al.*, 2010; Torrisi *et al.*, 2013). The target composition, optimal thickness, density, and microscopic structure influence the plasma production in terms of ion components, temperature and density of the plasma, and fluid dynamic evolution during the laser–plasma interaction (Torrisi, 2014*a*).

In particular, the use of graphene, acting as doping species, alters the polymer properties, for example, enhancing the absorption coefficient of the incident laser at particular wavelength bands, modifying the electrical and thermal conductance and enhancing the mechanical strength to compression and traction (Torrisi *et al.*, 2015*b*). In this context targets based on ultra-high-molecular-weight-poly-ethylene (UHMWPE) have been investigated as pure and as enriched by carbon–graphene in order to study the effects produced by laser irradiation and the consequent properties of the non-equilibrium generated plasma. The interest in this material comes from the possibility to use it as a source of high concentration of energetic proton and carbon ions. The accelerated carbon and ion beams extracted from plasma, in fact, play an important role in different scientific fields, from the microelectronics to medicine, from nuclear reactions to astrophysics, and from biology to chemistry (Schillaci *et al.*, 2014).

In this paper, we have prepared UHMWPE composites containing graphene at different doping concentrations and investigated their properties under high-intensity infrared (IR) pulsed laser irradiating. Both thick and thin foils were investigated in high vacuum. The mechanical strength of the material (PE with graphite) was secured to withstand the high radiation pressure acting on the thin foils during experiments of target-normal-sheath-acceleration (TNSA) regimes occurring at laser intensities of the order of 10^{18} W/cm^2 at which pressures higher than 10 GPa can be produced (Noack *et al.*, 1998). Measurements performed at low laser intensity, of the order of 10^{10} W/cm^2 were also carried out permitting to investigate the effects of prepulses of main *fs* giant pulses incident on the solid target. Prepulses play an important role on the laser transmission in undercritical plasma, on the laser interaction with the plasma gradients and on the laser reflection at the critical plasma density. Prepulses may induce self-focusing effects, with generation of hot electrons and production of filamentations and consequent induction of non-linear effects enhancing exponentially the directional ion acceleration process (Torrisi *et al.*, 2008; Chin *et al.*, 2011).

2. MATERIALS AND METHODS

UHMWPE has a density of 0.93 g/cm^3. PE is characterized by a C–H chemical bonding of 3.7 eV, while graphene by a C–C chemical bond of about 285 eV. The UHMWPE composites were prepared as follows. Graphene nanoplatelets (GNPs) were produced by LPE of highly ordered pyrolitic graphite (HOPG) via sonication in isopropanol using an ultrasonic bath (Soltec SONICA 1200 M, 160 W peak power) for 2 h [see (Messina *et al.*, 2016) for further details]. The solutions were prepared starting from a volume concentration of 0.5 mg/ml of HOPG in isopropanol and were stable in time. To embed the GNPs, the PE samples (10 × 20 mm^2 surface and 1 mm thickness) were placed on a hot plate at 150 °C and different amounts of GNPs solution, namely 3, 6 and 12 ml, were drop cast on the PE surface. Indeed, for common commercial high-density PE the softening point is typically in the range 120–150 °C. Under these conditions, it favors the blend of graphene to the polymer. After the solvent was evaporated, the samples were cooled down to room temperature and analyzed. The pure UHMWPE sheets in visible light appeared translucent, while the UHMWPE + GNPs composite appeared black colored (see Figure 1b).

Spherical gold nanoparticles (Au NPs) with an average size distribution of 100 nm, prepared by laser according to the literature (Torrisi *et al.*, 2015*b*), were employed to be embedded in PE containing grapheme, at a concentration of 1%

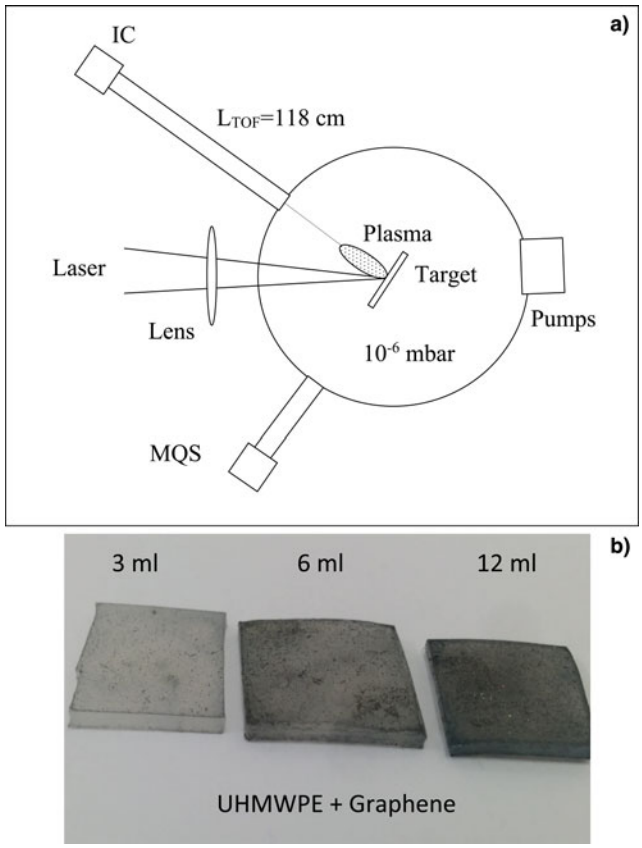

Fig. 1. Scheme of the used experimental setup (a) and photographs of the UHMWPE (white) containing, from left to right, 3, 6, and 12 ml graphene microparticles (black).

https://doi.org/10.1017/S0263034617000179 Published online by Cambridge University Press

in weight. The aim of these samples was that to enhance the electron density of the sample and, consequently, that of the laser-produced plasma when laser–matter interaction occurs.

A first optical characterization of the polymer composites was carried out by absorption measurements in the visible – near-IR as a function of the doping concentration (3, 6, and 12 ml). The investigations were performed with an XploRA PLUS micro-spectrometer, exploiting the halogen lamp embedded in the microscope as a light source in the 400–1000 nm range. The light was slightly focused on the sample with a condenser and the transmitted component gathered with a 10× microscope.

A linear array optical spectrometer (HoribaJobin Yvon VS140), with a resolution of 1–2 nm, was employed for absorption measurements in the prepared samples for wavelengths in the visible range and near UV and IR regions (250–1000 nm).

The extinction coefficient in cm^{-1} of the sample was evaluated by using the Lambert–Beer law:

$$\mu(\lambda) = \left(\frac{1}{\Delta x}\right) \ln\left[\frac{I_0(\lambda)}{I_T(\lambda)}\right], \quad (1)$$

where λ is the wavelength, Δx is the foil thickness, I_0 the intensity of the incident light, and I_T the intensity of the transmitted light.

Raman spectroscopy was performed in air and at room temperature by using the spectrometer equipped with a confocal microscope and a Peltier-cooled CCD (charge-coupled detector) in a backscattering configuration. Spectra were excited using the 638 nm line from a solid-state laser and integrated for 120 s, using a ×50 long working distance microscope objective. In order to prevent laser-induced damage or heating, measurements were carried out with a reduced laser power (1.8 mW on the illuminated area of 2.0 μm^2). Spectra from several random positions on each specimen were collected taking into account of the possible spatial non-homogeneity of the samples.

Morphological investigation of the prepared targets was performed using the optical and the electronic (SEM) microscopy.

A Nd:YAG laser, operating at 1064 nm, 3 ns pulse duration, single pulse or 1–10 Hz repetition rate, intensity of 10^{10} W/cm^2, max pulse energy of 300 mJ, and focalized laser spot of 0.5 mm^2 was employed to interact with the polymer surface in a vacuum chamber at 10^{-6} mbar pressure. The laser incident angle was 45° and the focusing lens was external to the vacuum chamber. Along the normal to the target surface an ion collector (IC) was placed at 118 cm distance in order to monitor the plasma properties using time-of-flight (TOF) measurements. A fast storage oscilloscope was employed to record the IC spectra (TekTronix TDS5104B, 1 GHz, 5 GS/s).

Mass quadrupole spectrometry (MQS) was employed coupled to the laser ablation in order to evince the ablated atomic and molecular species removed during the laser–matter interaction. MQS has a mass range 1–200 amu and a sensitivity lower than 1 ppm (part per million).

Figure 1a shows a scheme of the experimental apparatus used to irradiate in vacuum the prepared targets, while Fig. 1b shows a photo of the three targets based on UHMWPE containing different concentrations of graphene before to be irradiated by laser in high vacuum.

3. RESULTS

Measurements of the extinction coefficient as a function of the wavelength, in the range 250–800 nm, for the different prepared targets, are reported in Fig. 2a. The plots indicate that the absorbance decreases exponentially with the wavelength and about linearly with the graphene concentration in the UHMWPE (a), showing high absorption in the near-UV region and low in the visible one, in good agreement with the literature data (Li *et al.*, 2008).

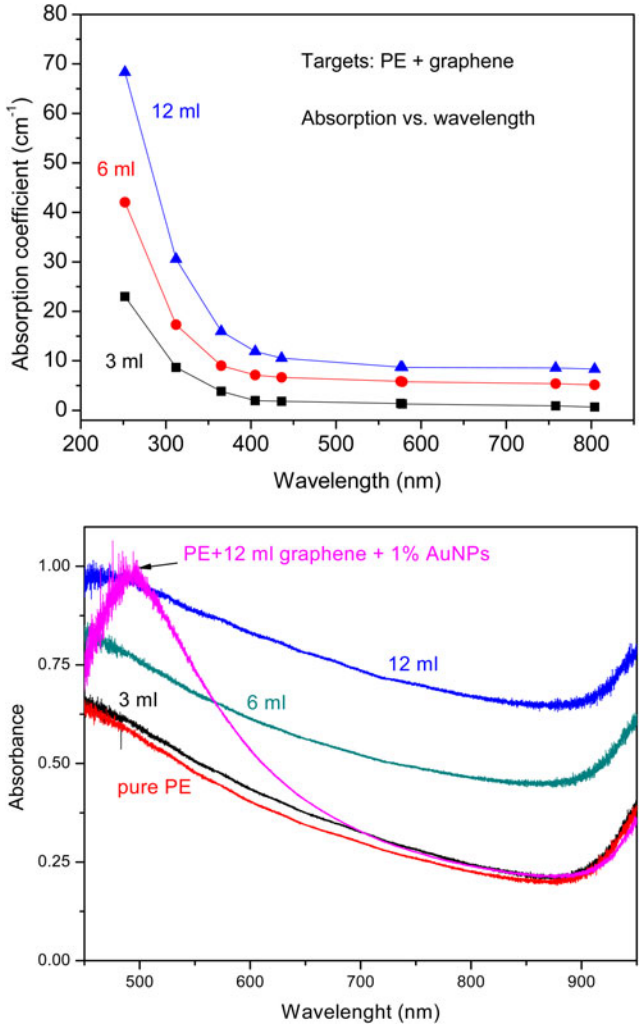

Fig. 2. Absorption coefficient versus wavelength for the different investigated polymers containing different graphene concentrations (a) and comparison at higher wavelengths with the absorbance in PE containing graphene and Au NPs (b).

https://doi.org/10.1017/S0263034617000179 Published online by Cambridge University Press

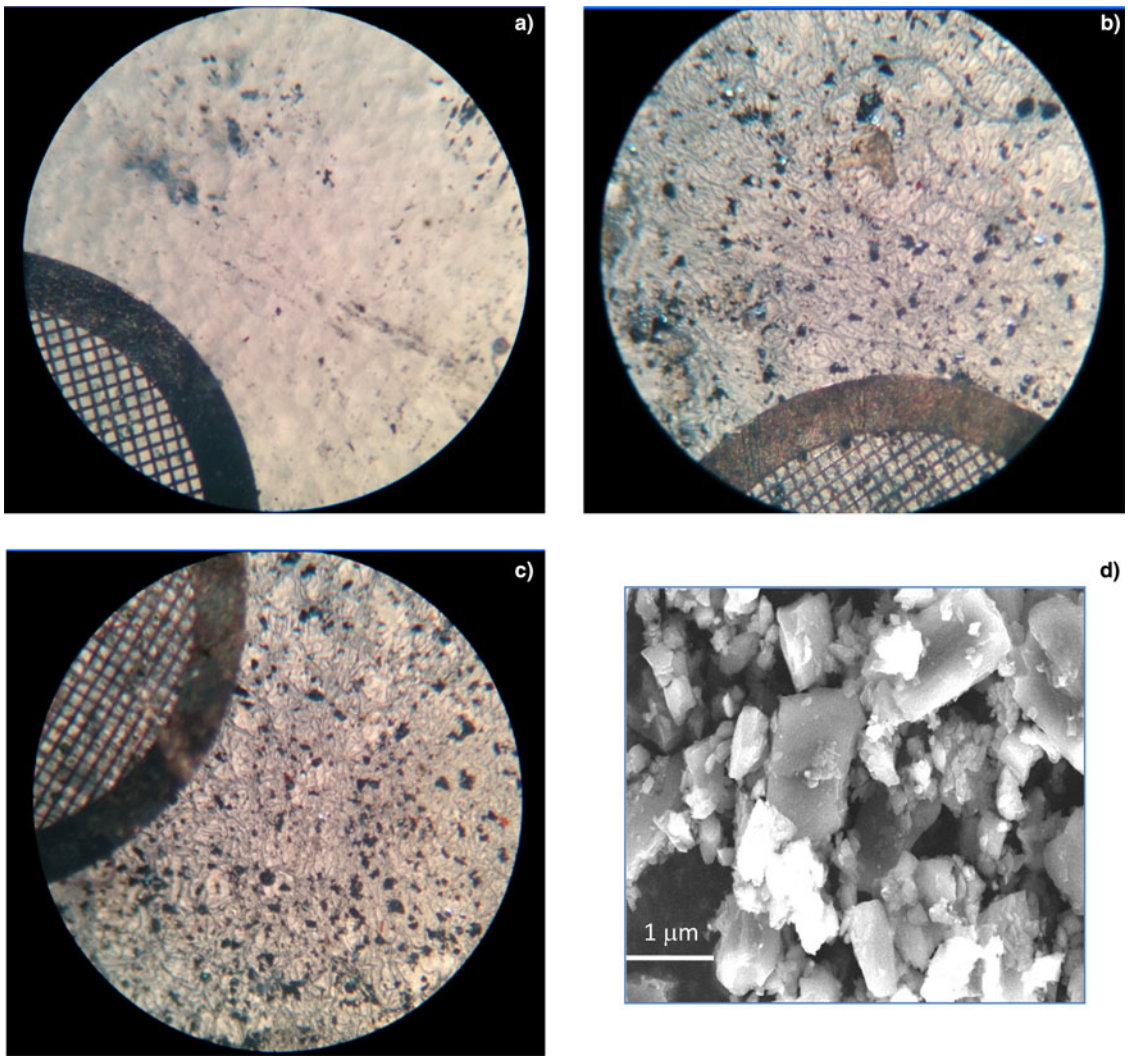

Fig. 3. Optical microscope images of the PE containing 3 ml (a), 6 ml (b), and 12 ml (c) of graphene and SEM image of the target containing the micrometric graphene particles (d).

Figure 2b reports a comparison of the optical absorption details in the prepared targets as a function of the wavelength, of the graphene concentration and of the presence of Au NP embedded in the polymer, for the wavelength range 450–950 nm, indicating an enhancement of the absorption coefficient with the filler content. An increment of absorption occurs toward 1000 nm, the laser wavelength, at which the fundamental harmonic of a Nd:YAG laser–solid matter interaction shows high absorption. Moreover, in presence of Au NP, due to their shape, size and environment, an absorption band is present in the wavelength range 400–600 nm, due to surface plasmon resonance absorption effects induced by the metal NPs (Garcia, 2012; D'Andrea *et al.*, 2015).

The optical measurements have demonstrated that high scattering process is observed for high concentration of graphene in PE in the visible region, decreasing with the concentration decrement of the graphene filler. The graphene micro and NPs, in fact, as thin micrometric foils randomly oriented in the polymer, act such as little reflecting surfaces inducing macroscopic scattering of the incident light, an effect reducing the transmission component at high concentration.

Figure 3 shows the optical microscope photos of the prepared samples at 3 ml (a), 6 ml (b), and 12 ml (c). The grid placed on the sample has 100 μm mesh size and indicates that the number of agglomerated graphene particles increases with their concentration in the polymer and that their maximum aggregation size is of the order of 100 μm.

Figure 4a reports the Raman spectra of the pristine HOPG (black line) and of the GNPs (red line) after exfoliation. Measurements were carried out after drop casting of the GNP solution on a silicon oxide surface and solvent evaporation. The main D, G, and 2D bands are visible (Ferrari *et al.*, 2006). The D band originates from the breathing mode of the sp^2 rings and shows up because of the presence of defects. On the GNPs we find it peaked at around 1335 cm^{-1} for 638 nm excitation, whereas it is negligibly small in the HOPG. The G-peak is due to bond stretching of sp^2 atoms

https://doi.org/10.1017/S0263034617000179 Published online by Cambridge University Press

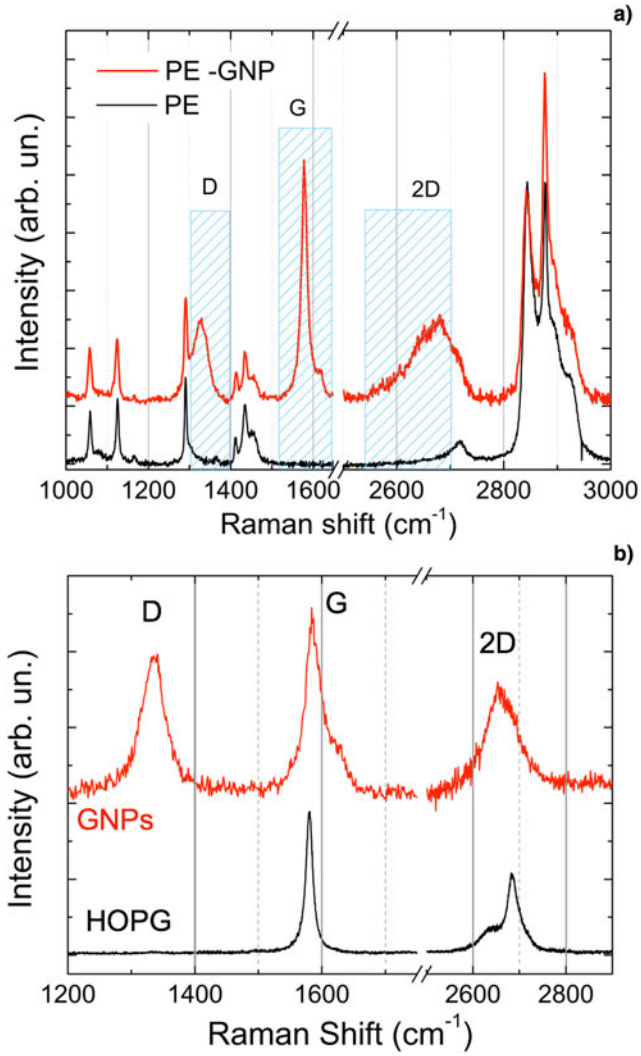

Fig. 4. (a) Raman spectra of HOPG (black) and of GNPs (red) produced by LPE. (b) Raman spectra of the PE sample (black) and of the PE-GNPs composite (red). The dashed boxes highlight the Raman bands of GNPs superposed to the peaks of PE.

and its position is found around 1584 cm^{-1} in both GNP and HOPG. The 2D band is the second order of the D peak and is located ~2650–2680 cm^{-1} for excitation at 638 nm. It is a single peak for single layer graphene and consists of two components in bulk graphite. For high purity micromechanically cleaved samples, the 2D band splits into several components and its shape allows one to distinguish among 2, 3, 4, 5, and >10 layers (bulk graphite) (Ferrari *et al.*, 2006). The Raman spectrum of graphene produced by LPE is more difficult to interpret. Staking faults, edge effects, strain and doping do not permit to unambiguously determine the number of layers present in a flake. In our spectra the 2D band of graphene platelets is different from HOPG, with a band peaked at 2653 cm^{-1} and consistent with graphene platelets containing few layers of graphene with random staking upon aggregation subsequent to IPA evaporation (Haar *et al.*, 2005).

Figure 4b reports the Raman spectra of the PE substrate (black line) and of the PE-GNP composite (red) prepared with 12 ml of GNP solution. Raman characteristic peaks of PE are identified in the 1000–1500 cm^{-1} region (CC stretchings and CH bending) and the high-energy region around 2900 cm^{-1} (CH stretching) (Schrader, 1989). A more detailed list of the vibration energies and of their mode assignment is reported in Table 1. The spectrum of the composite shows the presence, in addition, of the characteristic Raman bands of GNPs (highlighted by dashed boxes).

These characteristic peaks increase in intensity with the graphene concentration, as expected. The downshift of the G peak position in the composite (1577 cm^{-1} in the composite against 1584 cm^{-1} in the GNPs) suggests the presence of compressive stresses in the composite (Ni *et al.*, 2008), that can be attributed to the stresses induced due to solidification shrinkage of UHMWPE. These observations suggest that the composite fibers are similar to that of the pristine polymer and that the melt mixture of the graphene with the PE–CH_2 chains should produce a macroscopic reinforcement of the material with the filler increment, according to the literature (Andrews & Weisenberger, 2008). Samples investigated after intense bombardment did not show any spectral fingerprint of the GNPs, suggesting that the entire surface layer has been removed by the laser radiation.

The MQS coupled to the laser ablation in high vacuum has permitted to control the main ablated masses in the range 1–200 amu. The analysis was performed as a first time observing the background residual gases in the vacuum chamber and successively, during the laser ablation at 1 Hz repetition rate, irradiating the bulk composite target (3 mm thickness) and subtracting the background signal. The main detected masses laser generated during the target ablation were: 2 (H_2), 12 (C), 14 (CH_2), 15 (CH_3), 26 (C_2H_2), 28 (C_2H_4), 39 (C_3H_3), 78 (C_6H_6), 104 (C_8H_8), and 128 ($C_{10}H_8$), in well agreement with the literature (Torrisi *et al.*, 2010).

Figure 5a reports a typical MQS spectrum relative to some investigated masses during the laser ablation of the PE composite with 12 ml graphene. Spectra were acquired fixing the

Table 1. *Position of the Raman peaks of PE and vibrational modes assignment (Schrader, 1989).*

Raman signal	Assignment
1060 cm^{-1}	Asymmetric C–C stretching, crystalline
1080 cm^{-1}	Asymmetric C–C stretching, amorphous
1125 cm^{-1}	Symmetric C–C stretching, crystalline
1165 cm^{-1}	Rocking CH_2, crystalline
1290 cm^{-1}	Twisting CH_2, crystalline
1366 cm^{-1}	Bending CH_2, crystalline and amorphous
1410 cm^{-1}	Wagging CH_2, crystalline
1435 cm^{-1}	Deforming CH_2 , crystalline
1465 cm^{-1}	Bending CH_2, crystalline and amorphous
2845 cm^{-1}	Symmetric stretching CH_2, crystalline
2877 cm^{-1}	Anti-symmetric stretching CH_2, crystalline

https://doi.org/10.1017/S0263034617000179 Published online by Cambridge University Press

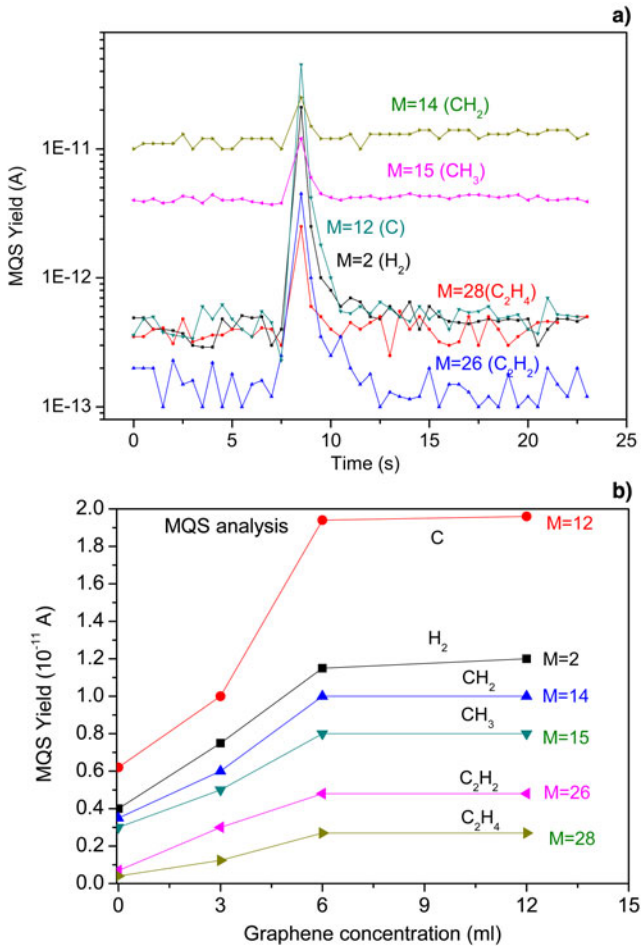

Fig. 5. Mass quadrupole yield versus time (a) and versus graphene concentration (b) for some fixed masses of interest.

masses of interest and starting with the scansion time during which a single laser shot was given and a mass pulse emission is recorded. In the plots the higher emitted masses in descending order were 12, 2, 14, 15, 26, and 28, corresponding to the emission of C, H_2, CH_2, CH_3, C_2H_2, and C_2H_4, respectively.

Figure 5b shows the MQS yield as a function of the graphene filler concentration for the different main ablated masses. Of course, as expected, the atomic carbon yield ($M = 12$) represents the stronger mass emission followed by the hydrogen ($M = 1$), which is contained in high quantities in the composite both as chemical bonded species and as absorbed gas.

The presence of Au NP in the polymer produces the emission of a mass peak at 197 amu, which yield growth proportionally to the Au NP concentration in the PE.

After the physical analyses of the composite characterization, the prepared targets were employed to study the laser–matter interaction process in vacuum. Using the Nd:YAG laser at 200 mJ, 1064 nm, 3 ns, 0.5 mm^2 spot, and single pulse to irradiate the four different targets at an incidence angle of 45°, plasma was monitored with the IC

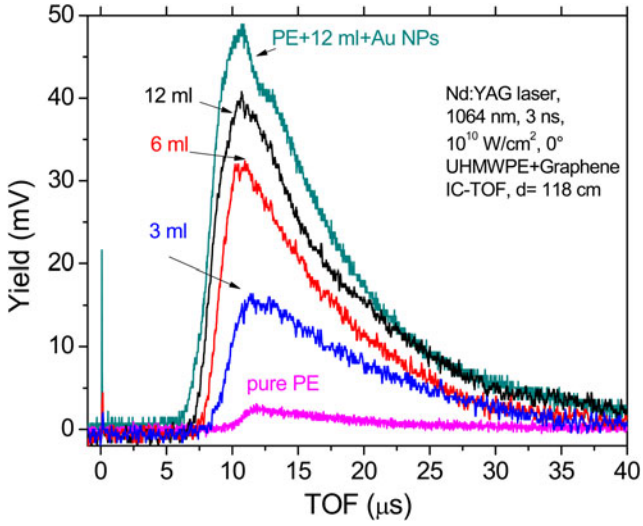

Fig. 6. IC-TOF spectra comparison in normal direction, detected at 118 cm distance from the target, for the different investigated advanced targets with graphene and with addiction of Au NPs.

detector placed at 118 cm distance from the target along the normal to the target surface. A comparison of the acquired TOF spectra is reported in Fig. 6.

Spectra show a fast photopeak due to photon detection, which permits to identify accurately the laser start time, and a larger and intense peak due to the ion detection giving the useful signal to evaluate the experimental TOF value, the mean ion velocity and the corresponding ion kinetic energy. With the used flight distance the ion peak does not permit a well separation of the protons from the carbon ions. Protons arrive to the IC at the start of the ion peak, while the carbon ions cover about all the peak areas with the convolution of their six charge states and with the presence of slower C_xH_y ionized groups. In pure PE, the faster protons have a TOF of about 9.4 μs, corresponding to a kinetic energy of 82 eV, while the faster carbon ions at about 12 μs, corresponding to a kinetic energy of about 600 eV, confirming a mean acceleration of about 100 eV/charge state and that the carbon ions may be ionized up to about six times.

Since accelerated particles have a Boltzmann distribution and because the ionization potentials increase with the ion charge state, the probability to generate C^{6+} is very low with respect to that to generate C^{1+}, in agreement with the Lotz ionization cross-sections (Shirkov & Zschomack, 1996). At the used relatively low laser intensity the main carbon charge states, in fact, are mainly the first four, in agreement with our previous measurements reported in the literature (Torrisi *et al.*, 2011), while the C^{5+} and C^{6+} charge states are almost negligible.

The ion yield in pure UHMWPE is low, with a maximum value extended up to about 3 mV, instead that relative to graphene embedded in the polymer increases to about 16, 32, and 41 mV for the graphene concentration of 3, 6, and 12 ml, respectively. In such synthesized targets, the proton TOF position decreases to about 8.5, 8.0, and 7.2 μs for the

https://doi.org/10.1017/S0263034617000179 Published online by Cambridge University Press

three graphene concentrations, respectively. This means that the proton acceleration increases with the graphene quantity up to 100, 114, and 140 eV from 3 to 6 ml up to 12 ml, respectively. Carbon ions also increase in energy from about 700 eV up to 870 eV, with energy proportional to their charge state. Practically the ion peak represents the deconvolution of the six charge states of the carbon ions contributes.

Thus, results demonstrate that the charge separation effects in the developed non-equilibrium plasma increase in density and temperature with the graphene concentration, producing an increment of the electric field driving the ion acceleration in the backward direction [backward-plasma-acceleration (BPA) regime]. This result confirms that the increment of the graphene concentration in the polymer enhances the electron density of the plasma and the laser absorption effect, producing more energetic plasma, according to the theory (Eliezer, 2002). Moreover, the further insertion of Au NPs at 1% in weight concentration with spherical shape and with 100 nm mean diameter, in the PE containing graphene enhances more the electron density of the target and its laser absorption coefficient, generating a further more hot plasma, as observed by the IC-TOF spectrum reported for comparison in Fig. 6, indicating proton acceleration up to 165 eV and carbon acceleration up to about 950 eV with a maximum carbon yield of 49 mV and a mean ion acceleration of about 160 eV per charge state.

The obtained results are confirmed by the optical absorption measurements of the prepared thin foils versus the wavelength (Fig. 2b). The maximum values of the absorption coefficients occur at low wavelengths, around 450 nm. Moreover, for comparison the same plot indicates that a stronger absorption is obtained embedding in the target also Au NPs at a concentration of 1% in weight. In the last case, the maximum absorption coefficient is shifted at about 500 nm wavelength.

Figure 7 shows the maximum plasma ion acceleration, in terms of maximum kinetic energy per charge state, and the carbon ion peak yield, as a function of the graphene filler concentration. Both quantities enhance with a similar growth law with the graphene content. The further insertion of Au NP in the polymer increases the process of ion acceleration because the electron density and the plasma temperature increases with the new composition of irradiated target resulting a major charge separation effects in the non-equilibrium plasma. Thus, the ion acceleration process increases from about 100 eV in the pure PE up to about 160 eV in the PE containing graphene at 12 ml and Au NP at 1% in weight, and the carbon yield enhances from about 3 mV up to 50 mV.

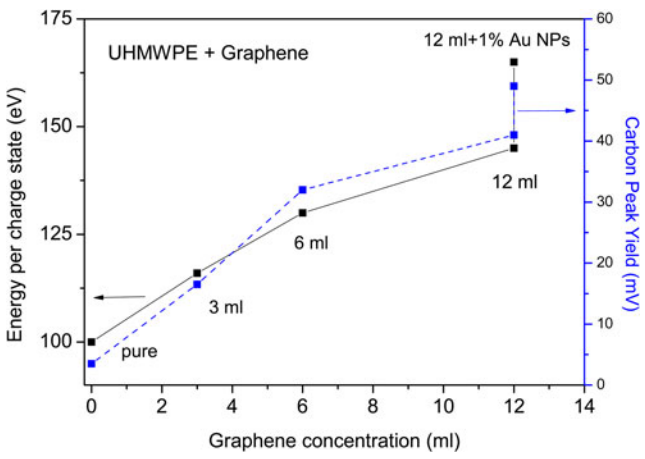

Fig. 7. Maximum ion kinetic energy per charge state and carbon peak yield versus graphene concentration with and without Au NPs.

We suspect that a similar enhancement or higher of ion energy and yield may be found in plasma generated by very high laser intensities ($\sim 10^{16-19}$ W/cm^2). The use of graphene micro and NPs as filler, in facts, increases the number of electrons accelerated by the laser light and the electron plasma density, consequently the particle interaction enhances and the temperature also producing higher ion acceleration, both for BPA than for TNSA regimes. Since carbon ions in pure PE are ionized mainly up to C^{4+}, as demonstrated by previously published ion energy distribution measurements (Torrisi *et al.*, 2011), it means that the plasma temperature, producing electron energies comparable with the C^{3+} ionization potential, should correspond to about 48 eV, as given by the ionizing potentials of the NIST database (NIST, 2017). However, the use of the advanced targets containing graphene and Au NPs generates high C^{6+} contribution enhancing the plasma temperature at least up to values comparable with the ionization potential of C^{5+}, which corresponds to 392 eV. Thus, the laser irradiation of the advanced targets should enhance the equivalent plasma temperature from the initial value of about 48 eV up to the value of about 392 eV.

IC was also used at different angles around the target normal direction. Such measurements demonstrated that the ion emission occurs mainly in the direction normal to the target surface with an angular aperture of about ±45°.

In the case of 12 ml graphene filler in PE, the number N of the total ions per laser shot, from C^{1+} up to C^{4+} accelerated along the normal direction, can be evaluated from the TOF spectra yield reported in Fig. 6, taking in consideration that the IC subtended solid angle is $\Delta\Omega = 1.4 \times 10^{-4}$ sr and assuming that the total emission occurs within a solid angle $\Omega = 3.14$ sr and the average charge state is $z = 2$, as follows:

$$N = \left(\frac{V \cdot \Delta t}{R \cdot ze}\right)\left(\frac{\Omega}{\Delta\Omega}\right) = \frac{41 \times 10^{-3}\text{V} \cdot 10 \times 10^{-6}\text{s}}{50\Omega \cdot 2 \times 1.6 \times 10^{-19}\text{C}} \cdot \frac{3.14\,\text{sr}}{1.4 \times 10^{-4}\,\text{sr}} = 5.75 \times 10^{14}\ \text{ions/laser shot}, \quad (2)$$

where V is the ion yield (V), Δt is the mean ion peak duration (s), R is the input resistance of the storage oscilloscope (50 Ω), and e is the electron charge (C).

https://doi.org/10.1017/S0263034617000179 Published online by Cambridge University Press

4. DISCUSSION AND CONCLUSIONS

The "advanced targets" used in this investigation are prepared in order to be irradiated by sub-ns high intensity lasers to generate hot and dense plasmas in vacuum from which protons and carbon ion beams can be extracted and accelerated at high energy. Although presented results are relative to the use of laser intensity of 10^{10} W/cm^2 to generate plasmas, the final goal is devoted to use intensities higher than 10^{16} W/cm^2, in different European laser facilities (PALS, CELIA, IPPLM, etc.), from which it is expected to obtain higher acceleration above 1 MeV per charge state.

The target composition was based on PE in order to have high hydrogen reserve to produce proton currents, to have high carbon concentration and to use a medium in which other elements, such as metallic nanoparticles (Au NP or others) or peculiar microstructures, such as graphene, can be embedded in order to modify the properties of the laser-generated plasma.

The obtained composite material (PE with and without Au NP) shows new optical properties with respect to the pristine PE, becoming high absorbent in the visible region with respect to the transparent pristine polymer. The mechanical properties are also modified making the material more resistant to tensile strength and rupture load, and providing useful characteristics to submit this material to high mechanical stresses, for example, to reduce the deformations due to radiation pressure during thin foils irradiated by high-intensity laser pulses. Also other physical properties, not investigated in this paper, are changed, such as, for example, the electrical and thermal ones, as reported in the literature (Potschke *et al.*, 2003). Such modifications concern also the color, the weight density, the electronic density, and the composition. The UHMWPE containing high graphene concentration is rich not only carbon, but also hydrogen, tanks to the capacity of carbon–graphene to absorb high hydrogen quantities, as demonstrated by our MQS analyses and as reported in the literature (Spyrou *et al.*, 2013).

In previous investigations, PE containing carbon multiwall nanotubes were studied and laser-generated plasma was produced in conditions similar to those used in the actual research. Results have demonstrated that the ion acceleration and the carbon yield is similar using graphene and carbon nanotubes; however, the use Au NPs enriching the electronic density of the PE+ graphene foils enhances significantly both the ion acceleration and the carbon yield in the laser-produced plasma (Torrisi *et al.*, 2016).

The advanced targets so produced and investigated are very useful to study the properties of the laser-generated plasma both at low and high intensities, intended to generate ion sources and high ion acceleration, respectively, which represents the final goal of this research. The study at intensity above 10^{19} W/cm^2 with *fs* TW lasers interacting with these advanced targets should permit to obtain plasmas with high electron density and relativistic energies, high plasma equivalent temperature, and high-charge separation both in TNSA and radiation–pressure–acceleration (RPA) regimes at which very high electric field can be developed to drive the ion directive acceleration. In both cases, the expected ion energy is higher than 10–20 MeV per charge state and the energy distribution should be withdrawn and not follow the Boltzmann distribution. The study at 10^{10} W/cm^2 with laser pulse duration of 3 ns, instead, permits to investigate on the laser prepulses generation to the successive giant laser pulse, which is more and more employed to produce a prepalsma where the successive laser pulse propagates and interacts with peculiar effects, such as self-focusing and filamentations (Wolowski *et al.*, 2004; Torrisi *et al.*, 2008). Moreover, this last is also useful in order to generate a laser ion source (LIS) for successive ion injection in traditional ion accelerators (Gammino *et al.*, 2004).

In the present contribution only a first study at low laser intensity was conducted, demonstrating that produced plasma enhances significantly the ion acceleration in the BPA regime thank to the amount of micrometric graphene particles embedded at different concentrations in the polymer. These advanced targets all have characteristics to produce high accelerated ions in carbon-hydrogenated plasmas and, as thick, to generate extractable high ion current using repetition rate lasers. The prepared advanced target can be used as high yield of proton and carbon ion source for many applications, such as LIS to inject pre-accelerated ions in superconducting cyclotrons of INFN-LNS in Catania (Italy) (Gammino *et al.*, 2004), production of 10–100 MeV proton and carbon ions for hadrontherapy according to aims of the ELIMED Project (Schillaci *et al.*, 2014), production of hot hydrogenated plasmas for astrophysical studies in the field of nuclear reactions induced in light nuclei and plasma Coulomb screening effects (Torrisi, 2014*b*), and inertial confinement fusion using composite pellets based on deuterium and tritium polymers containing high carbon nanoparticles (CNP) concentrations (Sang *et al.*, 2005).

Work is in progress in order to irradiate thin foils (1–50 μm in thickness) based on UHMWPE containing CNP and Au NP with TW *fs* lasers in the TNSA regime.

ACKNOWLEDGEMENTS

This research was supported by University of Messina Research & Mobility 2016 Project (project code RES_AND_MOB_2016_TORRISI). Authors thank the Nuclear Physics Institute of Rez (Czech Republic) as the research has been supported by project No. P108/12/G108.

REFERENCES

Andrews, R. & Weisenberger, M.C. (2008). Carbon nanotube polymer composites. *Curr. Opin. Solid State Mater. Science* **8**, 31–37.

Balandin, A.A. (2011). Thermal properties of graphene and nanostructured carbon materials. *Nat. Mater.* **10**, 569–581.

https://doi.org/10.1017/S0263034617000179 Published online by Cambridge University Press

Balandin, A.A., Ghosh, S., Bao, W., Calizo, I., Teweldebrhan, D., Miao, F. & Lau, C.N. (2008). Superior thermal conductivity of single-layer graphene. *Nano Lett*. **8**, 902–907.

Bolotin, K.I., Sikes, K., Jiang, Z., Klima, M., Fudenberg, G., Hone, J., Kim, P. & Stormer, H. (2008). Ultrahigh electron mobility in suspended graphene. *Solid State Commun*. **146**, 351–355.

Bonaccorso, F., Sun, Z., Hasan, T. & Ferrari, A.C. (2010). Graphene photonics and optoelectronics. *Nat. Photonics* **4**, 611–622.

Chin, S.L., Wang, T.J., Marceau, C., Wu, J., Liu, J.S., Kosareva, O., Panov, N., Chen, Y.P., Daigle, J.F., Yuan, S., Azarm, A., Liu, W.W., Seideman, T., Zeng, H.P., Richardson, M., Li, R. & Xu, Z.Z. (2011). Advances in intense femtosecond laser Filamentation in air. *Laser Phys*. **22**, 1–53. Pleiades Publishing Ltd.

D'Andrea, M., Irrera, A., Fazio, B., Foti, A., Messina, E., Maragò, O.M., Kessentini, S., Artoni, P., David, C. & Gucciardi, P.G. (2015). Red shifted spectral dependence of the SERS enhancement in a random array of gold nanoparticles covered with a silica shell: Extinction versus scattering. *J. Opt*. **17**, 114016.

Eliezer, S. (2002). *The Interaction of High-Power Lasers with Plasmas*. Bristol: *IOP Publishing*.

Ferrari, A.C., Meyer, J.C., Scardaci, V., Casiraghi, C., Lazzeri, M., Mauri, F., Piscanec, S., Jiang, D., Novoselov, K.S., Roth, S. & Geim, A.K. (2006). Raman spectrum of graphene and graphene layers. *Phys. Rev. Lett*. **97**, 187401.

Gammino, S., Torrisi, L., Ciavola, G., Andò, L., Celona, L., Maciagli, S., Krasa, J., Laska, L., Pfeifer, M., Rohlena, K., Mezzasalma, A.M., Gentile, C., Picciotto, A., Wolowski, J., Woryna, E., Badziak, J., Parys, P., Hitz, D. & Shirkov, G.D. (2004). The electron cyclotron resonance coupled to laser ion source for charge enhancement experiment: Production of high intensity ion beams by means of a hybrid ion source. *J. Appl. Phys*. **96**, 2961–2968.

Garcia, M.A. (2012). Surface plasmons in metallic nanoparticles: Fundamentals and applications. *J. Phys. D: Appl. Phys*. **45**, 389501.

Haar, S., El Gemayel, M., Shin, Y.Y., Melinte, G., Squillaci, M.A., Ersen, O., Casiraghi, C., Ciesielski, A. & Samori, P. (2005). Enhancing the liquid-phase exfoliation of graphene in organic solvents upon addition of N-octylbenzene. *Sci. Rep*. **5**, 16684.

Hasan, T., Sun, Z., Wang, F., Bonaccorso, F., Tan, P.H., Rozhin, A.G. & Ferrari, A.C. (2009). Nanotube–polymer composites for ultrafast photonics. *Adv. Mater*. **21**, 3874–3899.

Kuilla, T., Bhadra, S., Yao, D., Kim, N.H., Bose, S. & Lee, J.H. (2010). Recent advances in graphene based polymer composites. *Progr. Polym. Sci*. **35**, 1350–1375.

Li, D., Müller, M.B., Gilje, S., Kaner, R.B. & Wallace, G.G. (2008). Processable aqueous dispersions of graphene nanosheets. *Nat. Nanotechnol*. **3**, 101–105.

Messina, E., Leone, N., Foti, A., Di Marco, G., Riccucci, C., Di Carlo, G., Di Maggio, F., Cassata, A., Gargano, L., D'Andrea, C., Fazio, B., Maragò, O.M., Robba, B., Vasi, C., Ingo, G.M. & Gucciardi, P.G. (2016). Double-wall nanotubes and graphene nanoplatelets for hybrid conductive adhesives with enhanced thermal and electrical conductivity. *ACS Appl. Mater. Interfaces* **8**, 23244–23259.

Nair, R.R., Blake, P., Grigorenko, A.N., Novoselov, K.S., Booth, T.J., Stauber, T., Peres, N.M. & Geim, A.K. (2008). Fine structure constant defines visual transparency of graphene. *Science* **320**, 1308.

Ni, Z.H., Yu, T., Lu, Y.H., Wang, Y.Y., Ping Feng, Y. & Shen, Z.X. (2008). Uniaxial strain on graphene: Raman spectroscopy study and band-gap opening. *ACS Nano* **2**, 2301–2305.

NIST. (2017). Atomic Spectra Database Ionization Energies Data, actual website 2017: http://physics.nist.gov/cgi-bin/ASD/ie.pl

Noack, J., Hammer, D.X., Noojin, G.D., Rockwell, B.A. & Vogel, A. (1998). Influence of pulse duration on mechanical effects after laser-induced breakdown in water. *J. Appl. Phys*. **82**, 7488–7495.

Novoselov, K.S., Geim, A.K., Morozov, S.V., Jiang, D., Katsnelson, M.I., Grigorieva, I.V., Dubonos, S.V. & Firsov, A.A. (2005). Two-dimensional gas of massless Dirac fermions in graphene. *Nature* **438**, 197–200.

Potschke, P., Bhattacharyya, A.R. & Janke, A. (2003). Morphology and electrical resistivity of melt mixed blends of polyethylene and carbon nanotube filled polycarbonate. *Polymer* **44**, 8061–8069.

Rafiee, M.A., Rafiee, J., Wang, Z., Song, H., Yu, Z.Z. & Koratkar, N. (2009). Enhanced mechanical properties of nanocomposites at low graphene content. *ACS Nano* **3**, 3884–3890.

Sang, X.M., Yang, X.J., Cui, Z.D., Zhu, S.L. & Sheng, J. (2005). Nano-SiO_2 doped polystyrene materials for inertial confinement fusion targets. *J. Macromol. Sci. B: Phys*. **44**, 237–248.

Schillaci, F., Anzalone, A., Cirrone, G.A.P., Carpinelli, M., Cuttone, G., Cutroneo, M., De Martinis, C., Giove, D., Korn, G., Maggiore, M., Manti, L., Margarone, D., Musumarra, A., Perozziello, F.M., Petrovic, I., Pisciotta, P., Renis, M., Ristic-Fira, A., Romano, F., Romano, F.P., Schettino, G., Scuderi, V., Torrisi, L., Tramontana, A. & Tudisco, S. (2014). ELIMED, MEDical and multidisciplinary applications at ELI-Beamlines. *J. Phys.: Conf. Ser*. **508**, 012010.

Schrader, B. (1989). *Raman/Infrared Atlas of Organic Compounds*. Weinheim: VCH. ISBN 3–527–26969-X.

Shahil, K.M. & Balandin, A.A. (2012). Graphene–multilayer graphene nanocomposites as highly efficient thermal interface materials. *Nano Lett*. **12**, 861–867.

Shirkov, G.D. & Zschomack, G. (1996). *Electron Impact Ion Source for Charged Heavy Ions*. Gottingen: *ViewegPubl*.

Spyrou, K., Gournis, D. & Rudolf, P. (2013). Hydrogen storage in graphene-based materials: Efforts towards enhanced hydrogen absorption. *ECS J. Solid State Sci. Technol*. **2**, M3160–M3169.

Torrisi, L. (2014*a*). Ion energy enhancement from TNSA plasmas obtained from advanced targets. *Laser Part. Beams* **32**, 383–389.

Torrisi, L. (2014*b*). Ion acceleration and D–D nuclear fusion in laser-generated plasma from advanced deuterated polyethylene. *Molecules* **19**, 17052–17065.

Torrisi, L., Calcagno, L., Giulietti, D., Cutroneo, M., Zimbone, M. & Skala, J. (2015*a*). Laser irradiations of advanced targets promoting absorption resonance for ion acceleration in TNSA regime. *Nucl. Instrum. Methods B* **355**, 221–226.

Torrisi, L., Caridi, F. & Giuffrida, L. (2011). Protons and ion acceleration from thick targets at 10^{10} W/cm^2 laser pulse intensity. *Laser Part. Beams* **29**, 29–37.

Torrisi, L., Ceccio, G. & Cutroneo, M. (2016). Laser-generated plasma by carbon nanoparticles embedded into polyethylene. *Nucl. Instrum. Methods Phys. Res. B* **375**, 93–99.

Torrisi, L., Cutroneo, M., Andò, L. & Ullschmied, J. (2013). Thomson parabola spectrometry for gold laser-generated plasmas. *Phys. Plasmas* **20**, 023106.

https://doi.org/10.1017/S0263034617000179 Published online by Cambridge University Press

Torrisi, L., Cutroneo, M. & Ceccio, G. (2015*b*). Effect of metallic nanoparticles in thin foils for laser ion acceleration. *Phys. Scr*. **9**, 015603.

Torrisi, L., Margarone, D., Laska, L., Krasa, J., Velyhan, A., Pfeifer, M., Ullschmied, J. & Ryc, L. (2008). Self-focusing effect in Au-target induced by high power pulsed laser at PALS. *Laser Part. Beams* **26**, 379–387.

Torrisi, L., Visco, A.M., Campo, N. & Caridi, F. (2010). Pulsed laser treatments of polyethylene films. *Nucl. Instrum. Methods Phys. Res. B* **268**, 3117–3121.

Wolowski, J., Badziak, J., Parys, P., Rosinski, M., Ryc, L., Jungwirth, K., Krasa, J., Laska, L., Pfeifer, M., Rohlena, K., Ullschmied, J., Mezzasalma, A., Torrisi, L., Gammino, S., Hora, H. & Boody, F.P. (2004). The influence of pre-pulse plasma on ion and X-ray emission from Ta plasma produced by a high-energy laser pulse. *Czech. J. Phys*. **54** (Suppl. C), C385–C390.

Yu, L.Z., Zhiming, T., George, P.S. & Dan, L. (2015). Scalable production of graphene via wet chemistry: Progress and challenges. *Mater. Today* **18**, 73.

Zeil, K., Kraft, S.D., Bock, S., Bussmann, M., Cowan, T.E., Kluge, T., Metzkes, J., Richter, T., Sauerbrey, R. & Schramm, U. (2010). The scaling of proton energies in ultrashort pulse laser plasma acceleration. *New J. Phys*. **12**, 045015.

https://doi.org/10.1017/S0263034617000179 Published online by Cambridge University Press